Microfluidic means of achieving attomolar detection limits with molecular beacon probes†

Christopher M. Puleo[a] and Tza-Huei Wang*[b]

Received 4th November 2008, Accepted 20th February 2009
First published as an Advance Article on the web 6th March 2009
DOI: 10.1039/b819605b

We used inline, micro-evaporators to concentrate and transport DNA targets to a nanoliter single molecule fluorescence detection chamber for subsequent molecular beacon probe hybridization and analysis. This use of solvent removal as a unique means of target transport in a microanalytical platform led to a greater than 5000-fold concentration enhancement and detection limits that pushed below the femtomolar barrier commonly reported using confocal fluorescence detection. This simple microliter-to-nanoliter interconnect for single molecule counting analysis resolved several common limitations, including the need for excessive fluorescent probe concentrations at low target levels and inefficiencies in direct handling of highly dilute biological samples. In this report, the hundreds of bacteria-specific DNA molecules contained in ~25 microliters of a 50 aM sample were shuttled to a four nanoliter detection chamber through micro-evaporation. Here, the previously undetectable targets were enhanced to the pM regime and underwent probe hybridization and highly-efficient fluorescent event analysis *via* microfluidic recirculation through the confocal detection volume. This use of microfluidics in a single molecule detection (SMD) platform delivered unmatched sensitivity and introduced compliment technologies that may serve to bring SMD to more widespread use in replacing conventional methodologies for detecting rare target biomolecules in both research and clinical labs.

1 Introduction

The development of microanalytical systems for biosensing is driven by advances in microfluidic control technologies for handling nano- to picoliter sample volumes.[1–3] However, the use of small sample volumes in these platforms also requires highly sensitive analyte detection schemes and it is the development and integration of these detection approaches, which remains one of the main challenges for the practical application of microfluidic devices.[4,5] Traditionally, laser-induced fluorescence (LIF) and methods for electrochemical detection provide the workhorse detection schemes for microanalysis, although recently there has been considerable progress in alternate detection techniques, such as, surface plasmon resonance (SPR), chemiluminescence, Raman, infrared, and absorbance-based detectors.[5,6] The original detection technique LIF is most often used in conjunction with micro-capillary electrophoresis (CE) platforms, and this combination of separation and sensitive fluorescence detection remains one of the most represented classes of analytical microsystems.[6]

In parallel to these micro-CE platforms several researchers concentrate on the development of target-specific, amplification- and separation-free fluorescent biomolecular detection methods.[7–17] In these methods, the confocal detection design of LIF enables ultrasensitive, single molecule detection (SMD), while several unique probe strategies, such as molecular beacons,[12,18,19] two-color coincidence detection,[7,9,10,13–15,20] or additional FRET or PET-based probes[8,11,16] facilitate specific molecular detection in a homogenous format. Although the sensitivity of LIF in detecting single fluorescent molecules yields infinitely low theoretical detection limits for biomolecular targets, the practical limitations of LIF-based SMD platforms are reported in the pM to fM range.[11,13,15,18]

These common detection limits stem from two main challenges. The first is that analysis of probe–target interactions is complicated by free probe molecules. Although it is desirable to use high concentrations of probe molecules in order to increase probe–target interaction rates and ensure target saturation in a reasonable time, high excess probe causes increased background that prevents enumeration of single molecule fluorescence. For instance, although self-quenching probes, such as molecular beacons or smart probes, exhibit low background signals, the concentration of such probes still has to be restricted to the sub-nanomolar level in order to facilitate detection of single molecules.[18] Previous attempts to deal with these complications include the use of fluorescent quenchers to suppress signal from unbound probe[21] or the use of nanocrystals in unique FRET pairings,[11] allowing for the use of increased probe concentrations to improve probe–target interactions. However, strategies such as these add cost and complexity to the assays and do not result in detection limits that breach the fM regime.

Secondly, nearly all of the successful applications of these SMD platforms utilize traditional means of analyte delivery, that is, fluorescently-labeled biomolecules are delivered to the focused laser observation volume through continuous flow within

[a]*Johns Hopkins University, Department of Biomedical Engineering, 3400N. Charles St., Clark Hall Rm. 123, Baltimore, MD, USA. E-mail: cpuleo@jhu.edu; Fax: +1-410-516-4771; Tel: +1-410-516-7576*
[b]*Johns Hopkins University, Departments of Mechanical Engineering and Biomedical Engineering, 3400N. Charles St., Latrobe Hall Rm. 108, Baltimore, MD, USA. E-mail: thwang@jhu.edu; Fax: +1-410-516-4316; Tel: +1-410-516-7086*

† Electronic supplementary information (ESI) available: Time course measurement of DNA adsorption to PDMS. See DOI: 10.1039/b819605b

a micro-capillary or microfabricated channel.[5,7,11,13–15] In this case, the potential for assay miniaturization is confounded by inefficient fluidic couplings, reliance on external pumping systems, and size mismatch between the observation volume and flow cell. Indeed, these drawbacks restrict the use of homogenous, single molecule probe strategies, relegating them to isolated, large sample volume platforms with low mass detection efficiency[5,13,15] However, use of a closed-loop, rotary pump[22] eliminates the extra fluid couplings associated with traditional SMD platforms and provides repeated, random sampling of probe–target interactions from nanoliter chambers[23] thus, enabling new analyte delivery schemes tailored for discrete, low-volume SMD assays and specific biosensing strategies.

Herein, we describe a microfluidic coupling to deliver and concentrate targets to nanoliter-sized SMD chambers[23] from otherwise undetectably low concentrations of sample DNA. In the design, a membrane-based, microfluidic evaporator serves as the input to a SMD rotary chamber and following solvent removal *via* pervaporation, a concentrated sample plug is transferred for probe–target hybridization and interrogation *via* single molecule fluorescence burst counting. Though simple in design and function this unique means of analyte delivery represents a powerful method to overcome the traditional limitations associated with SMD within microfluidic systems. First, the required fluorescent probe concentrations for efficient probe–target interactions within the highly dilute samples are minimized through target pre-concentration, thus diminishing the effect of background fluorescent events. In addition, direct measurements are made from clinically relevant microliter sample volumes through the use of micro-evaporators as unique interconnects between the dilute DNA samples and the nanoliter-sized SMD rotary chamber. Furthermore, application of this microfluidic detector–concentrator combination is shown to be ideal due to both the relatively gentle conditions necessary for solvent removal and the highly controlled rate of evaporation.

Indeed, desktop analyte concentration by solvent removal remains a mainstay in clinical and biological labs, as centrifugal and rotary evaporators are commonly used for nucleic acid preparation steps,[6] during which DNA from large tissue samples are isolated into manageable sample sizes. This simple step has served as an enabling technique for the most highly sensitive, desktop biomolecular assays, such as polymerase chain reaction (PCR) and microarrays for decades. Still, evaporation in microdevices is most often looked upon as a nuisance[24,25] and utilization of solvent removal for practical applications remains rare.[26–28] Here, the practicality of coupling micro-evaporation with highly sensitive microanalytical platforms is demonstrated by decreasing the relative limit of detection of a common molecular beacon probe by over four orders of magnitude, thus surpassing previous limits set by more complex SMD probe schemes[11,21] through a purely microfluidic means.

2 Materials and methods

Microdevice design

The devices, shown in Fig. 1A, were prepared as two layer PDMS (Sylgard 183) on glass using multilayer soft lithographic techniques (MSL),[29] as described previously.[23] Fig. 1B depicts the

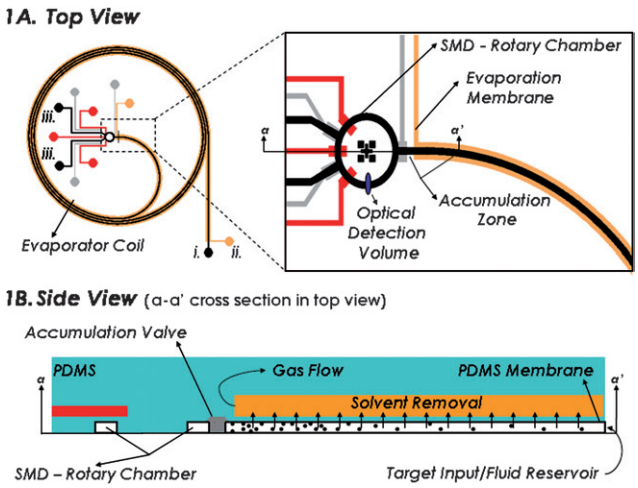

Fig. 1 **(A)** Schematic of the combined micro-evaporator/rotary SMD microdevice. The control layer (lighter grey) shows the evaporation membrane, rotary pump, and isolation valves. Target accumulation is accomplished by solvent removal from the fluidic layer (black, inlet labeled i.) through the pervaporation membrane (inlet labeled ii.). Following target accumulation the concentrated sample plug is transferred to the SMD rotary chamber for probe hybridization and detection; probes and hybridization buffer are introduced through separate inlets (labeled iii.). **(B)** Side view of the operating micro-evaporator, prior to sample transfer into the detection chamber. Solvent removal through the pervaporation membrane must be compensated by convection from the sample reservoir, while actuation of the accumulation valve enables target collection at the dead end.

operation principles for pervaporation-based concentration,[25,30] as described in the Results section. The cross-sectional dimensions of the fluidic channel measured 100 μm wide by 12 μm high, while the top, evaporation layer overlapped at slightly larger dimensions of 200 μm wide by 50 μm high. The PDMS membrane separating the two layers ranged from 20–30 μm with slight device-to-device variation. The sample inlet (labeled i.) of the fluidic channel was connected to a sample reservoir using 0.02″ tygon tubing (Cole-Parmer) fitted with blunt-end, steel needle tips (McMaster-Carr, gauge 23). Access holes were punched in both layers using needle tips enabling device loading either directly from the tubing reservoir or gel-loading pipette tips for samples volumes as low as 0.1 μL.

The SMD rotary chamber had dimensions of 1 mm loop diameter, 12 μm depth, and 100 μm width, while the intersecting valve control dimensions were 200 μm width by 50 μm depth. Fig. 2 depicts target accumulation at the inlet of this chamber during device operation and the loading steps for interrogation, with further description in the Results section. The three valves trisecting the rotary chamber had two functions. First, they served to segment the chamber into multiple compartments to enable loading of multiple fluidic samples (Fig. 2D and E). Second, actuation of the three valves in alternating patterns enabled peristaltic actuation of the four nanoliter sample within the chamber, creating a microfluidic rotary pump (Fig. 2F).[22] All valve components of the device were primed with filtered water, controlled using the same needle tip connections used above, and pressurized with separate compressed air sources. Actuation sequences were programmed using an array of solenoid valves

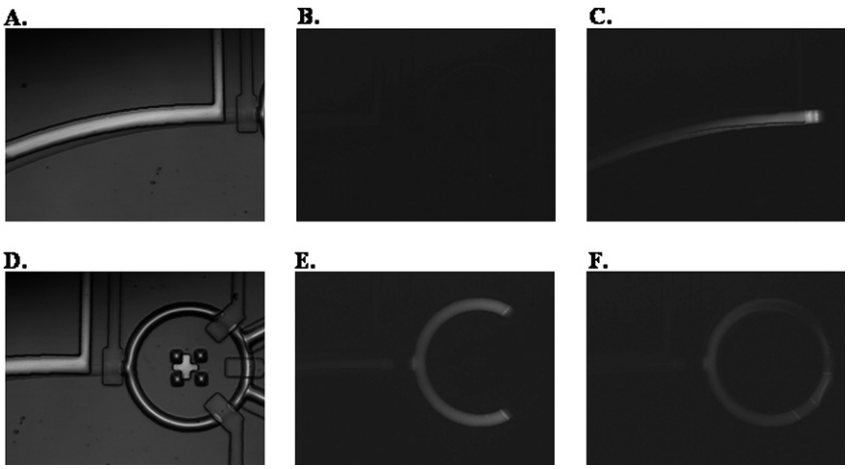

Fig. 2 **(A and B)** Photo- and fluorescence micrographs of the accumulation zone just prior to the closed accumulation valve at time 0 after loading the evaporator coil with 500 nM fluorescently-labeled DNA sequences. **(C)** Fluorescence micrograph showing target accumulation after 6 hours of evaporation in the 1000 mm membrane pervaporator with 20 PSI nitrogen pressure and at room temperature. **(D)** Photomicrograph of the SMD rotary chamber just prior to sample injection with valves bisecting the chamber into analyte (left three-quarters) and probe/buffer (right one-quarter) compartments. **(E)** Accumulated model target from Fig. 2C is injected into the rotary chamber along with DI water in the probe/buffer section. **(F)** Mixing of the contents shown in Fig. 2E for 1 s using the rotary pump at 10 Hz, mixing at the 100 Hz pump rate was complete within 5 s (data not shown).

(Asco) and a Visual Basic (Microsoft) interface for an electrical switchboard (Agilent). Rotary actuation provided efficient mixing of the concentrated nanoliter plug with molecular probes and reaction buffers and enabled downstream recirculation for SMD analysis of specific biomolecules that accumulated during pervaporation.[23]

The microdevices were coupled to a custom confocal fluorescence spectroscopic system by positioning the chip into a piezo-actuation stage capable of sub-micron resolution (Physik Instrumente) in order to focus the optical probe volume at the channel midpoint.[23] A HeNe laser (633 nm, 25-LHP-151-249, Melles Griot) was expanded to match the back aperture of the focusing objective (100×, 1.4 N.A., UPlanFl, oil immersion, Olympus) after reflection by a dichroic mirror (51008 BS, Chroma Technology). During experiments the laser power was attenuated to ~100 μW by a neutral density filter before entering the objective and the beam was focused 6 μm into the channels, using the water–glass interface as a reference point. Emitted fluorescence was collected by the same objective, passed through a 50 μm pinhole (PNH-50, Melles Griot), and focused onto an avalanche photodiode (APD, SPCM-AQR-13, PerkinElmer) after band pass filtering (670DF40, Omega Optical). Acquisition software, written in Labview (National Instrument), and a digital counter (National Instrument) were used to collect data from the APDs. Threshold fluorescence values were determined by evaluating no target control samples, while single molecule events were defined by bursts within non-filtered data streams, where photon counts exceeded this preset threshold. Integration time for photon binning was set at 1 ms for all peak counting experiments, unless otherwise stated.

Pervaporation-induced flow measurement

Previous groups described pervaporation-induced flow, determining velocity distributions within the microchannel by assuming a constant volumetric flow rate of water through the PDMS membrane.[25,30] In our study, bulk evaporation measurements were taken by evaluating the average displacement of the sample meniscus inside the reservoir tubing. In addition, time dependent fluctuations of the maximum pervaporation-induced flow rate was determined at the start of the membrane using an adaptation of a method previously described by our lab,[31] in which the average duration of single molecule fluorescence bursts represent the flow rate dependent transit time of molecules/particles passing through the optical detection volume. In these measurements, fluorescent bursts were measured using samples of 6×10^8 particles mL^{-1}, 0.1 μm tetraspec fluorescent beads (Molecular Probes) and the signal integration time for photon binning was set to 0.1 ms. Prior to burst analysis all flow measurement data was smoothed using the Lee Filter algorithm in order to provide more meaningful burst durations in low flow rate conditions.[32,33] Stability of the evaporation-induced flow was measured over time by monitoring fluorescent bursts in 100 s intervals, immediately following sample loading and commencement of gas flow within the top, evaporation channel. The effect of several operational parameters on flow rate control and stability were investigated, including evaporation chamber length, nitrogen flow rate, fluidic channel back-pressure, and device temperature.

Molecular beacon (MB) probe and single molecule detection

A DNA-MB (5′-Cy5-CATCC**GCTGCCTCCCGTAGGAG** T-G-BHQ2-3′) was synthesized by Integrated DNA Technologies (IDT) with the probe sequence (indicated in bold) complementary to a conserved region of the 16S rRNA in a wide-range of bacteria.[34] Complementary DNA oligonucleotides (IDT) were diluted in water and then loaded to fill a coiled, 1000 mm long channel. Pressurizing the reservoir tubing allowed complete dead-end filling, and maintained channel shape and sample continuity even at high nitrogen flow rates within the evaporation channel. For all experiments, both the back-pressure of the

fluidic channel and the nitrogen pressure were kept equal (25 PSI for MB experiments), while control valves were actuated at 35 PSI to maintain closure. Control hybridization experiments were carried out without evaporation by loading the rotary pump with known concentrations of target DNA in water, then hybridizing the targets with MB probes (10 pM final concentration) loaded with hybridization buffer, in the second input. Prior to all hybridization experiments the microdevice was rinsed with a detergent (0.1% SDS) for 10 min and filtered water for 1 h, prior to drying in an oven overnight. The hybridization buffer was loaded with the probes to yield concentrations of 10 mM phosphate buffer (pH 7.8) and 900 mM NaCl after mixing and dilution with the target sample. The rotary pump was run at 100 Hz for 15 s upon loading of the rotary chamber with targets and probes, prior to heating the chip to 80 °C using a flatbed thermocycler (custom Labnet MultiGene II) for 5 s and incubation at room temperature for 1 h. After hybridization, the rotary pump was run at 100 Hz to recirculate sample through the optical probe volume and perform fluorescence burst counting for DNA detection within the four nanoliter chamber.[23] Upon determining the detection limit under these conditions, five incubation times were examined (5, 10, 15, 20, 30 min) to ensure optimal hybridization in subsequent concentrator experiments. The hybridization study was then repeated after accumulating DNA targets from samples at different concentrations using the evaporation channel, allowing determination of the efficacy of the combined evaporator–SMD microdevice. It is important to note that DNA targets were prepared from a 1 μM stock solution in 1× TE buffer by diluting to the experimental concentrations of 5–500 aM in purified water. Thus, these extreme dilutions rendered the effects of the original buffer concentration negligible, even after relatively large amounts of solvent removal.

3 Results and discussion

Principle and operation of the microfluidic device

As shown in Fig. 1A and B, solvent in the bottom, fluidic layer pervaporated through the thin PDMS membrane separating this sample layer and the evaporation channel. Evaporated solvent was replaced through convection from a sample reservoir (labeled i.), while dry nitrogen was flown through the evaporation channel (labeled ii.) to maintain a more constant driving force for pervaporation throughout the device. In our design, accumulation of analyte was accomplished through the incorporation of a MSL valve (accumulation valve) to interrupt the convective flux from the reservoir. The fluidic and evaporation channels were coiled from this dead-end valve, allowing fabrication of devices with pervaporation membranes from 5 to 2000 mm in length. The reversible, MSL valve allowed manipulation of the concentrated sample plugs, which form after solvent removal and solute accumulation. Fig. 2 shows the accumulation of model, FAM-labeled, single stranded DNA (500 nM, 23 nt sequence, IDT) at this dead-end valve (Fig. 2C), followed by subsequent release of the valve and transfer of the concentrated nanoliter-sized sample plug to a downstream SMD rotary chamber (Fig. 2E). Images of the model fluorescent targets were taken using a 5× objective (Olympus BX51) and a cooled CCD camera (RetigaExi, QImaging Corporation) at 2 s exposure time. In MB experiments, probes and hybridization buffer were then loaded into the remaining portion of the rotary chamber for subsequent mixing with the concentrated sample plug (Fig. 2F) and recirculating SMD.[23]

Device characterization

As discussed previously, the compensating flow from the fluid reservoir must equal the volumetric flow rate achieved by the pervaporation membrane.[30] Therefore, the effectiveness of coupling the concentrator to the SMD rotary chamber is dependent on the magnitude and stability of the volumetric flow rate due to evaporation, which were measured both by quantifying average burst durations of polymer beads just upstream of the channel entrance and by observing the motion of the meniscus within the tubing reservoir. Fig. 3 shows average evaporation rates within the microdevice after altering various operational parameters, including applied pressure, temperature, and evaporation membrane length. The increasing evaporation rates with nitrogen pressure (Fig. 3A) were likely attributable to the faster nitrogen flows within the device, which act to purge water vapor and minimize diffusive boundary layers across the pervaporation membrane. In all experiments back-pressure applied to both the sample channel and nitrogen flow channels were increased simultaneously and increasing sample pressure alone had little effect on the non-negligible evaporation rates with zero applied nitrogen flow (data not shown). However, this effect of nitrogen flow on evaporation rate is limited, as higher flow rates eventually result in constant driving forces for evaporation within the device, and interfaces between device layers often fail at back-pressures approaching 40– 50 PSI. Still, several additional methods exist for increasing evaporation rates and thus the efficacy of the combined concentrator–detector. Fig. 3B shows the evaporation rates from a 1000 mm pervaporator when held at various temperatures using a flatbed thermocycler, with a maximum rate of ~120 nL min^{-1} at 80 °C, while Fig. 3C shows rates from microdevices held at room temperature (~25 °C) with varying evaporation membrane lengths. Importantly, while not fully optimized in this report, the dependence of evaporation rates on multiple device parameters enables concentration approaching the hundreds of microliters per hour rates associated with desktop evaporators.[35] In addition, elimination of any air–liquid interface in the membrane-based microfluidic evaporator eradicates spurious convective flows or bumping, which may cause sample-loss or cross contamination in alternative macro- or micro-evaporator designs.[27,36] Furthermore, the low thermal mass within the micro-evaporator permits isothermal conditions gentle enough to preserve the activity of biological species, while integration of the evaporator with MSL control technologies allows direct coupling of the analytical component of the microdevice, thereby maximizing sensitivity.

Fig. 3D shows a time trace of the average fluorescent burst duration of fluorescent beads within a 1000 mm, coiled pervaporation chamber immediately following the start of nitrogen circulation within the top channel. Unlike the bulk evaporation data presented thus far, the single particle measurements show large transient sample flows and non-negligible latency times (up to 15 min) due to vibrations of the coiled membrane at low applied nitrogen pressures. The large sample flow rates (short

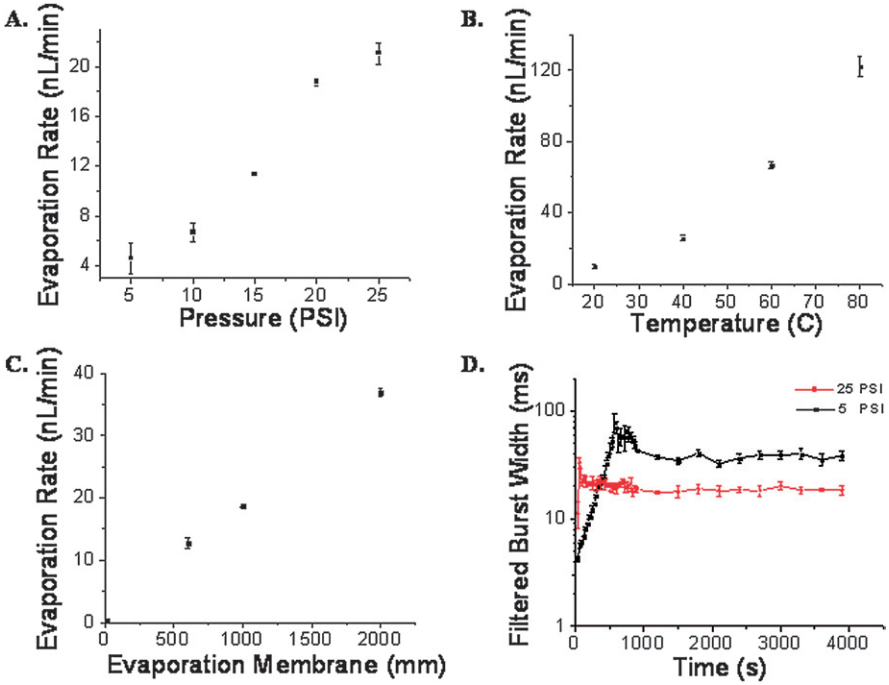

Fig. 3 **(A, B, and C)** Bulk evaporation rates *versus* evaporation pressure (A), microdevice temperature (B), and evaporation membrane length (C). Pressure data were taken using a 1000 mm membrane at room temperature. Temperature data were taken using a 1000 mm membrane at 25 PSI, while evaporation length data were taken at room temperature and 25 PSI. **(D)** Time trace of the measured fluorescent burst duration of tetraspec beads at the start of the evaporation channel at two different evaporation pressures (25 and 5 PSI). Large fluctuations at low pressure are due to evaporation membrane vibration upon initiation of nitrogen flow. Points for A, B, and C are mean evaporation rates from a single device after three separate 2 h measurements ± standard error.

burst durations) observed immediately after commencement of nitrogen flow is followed by sample flow cessation (long burst durations), which is caused by reflection of the vibration induced sample convection at the dead-end or accumulation valve. After damping of this transient flow, burst durations reach a stable value, which persist throughout device operation. Increasing the back-pressure applied to the fluid and gas channels (25 PSI) lead to faster damping of this transient flow and steady evaporation within seconds, thus allowing device operation with minimal latency times.

Attomolar detection of DNA targets with MBs

Fig. 4 shows the fluorescence burst data for control MB hybridization experiments within the microdevice, without the use of the evaporator. In bulk studies, dual-labeled, hairpin probes commonly increase in fluorescence intensity from 10–100 fold upon hybridization to complementary targets.[37] This signal-to-background ratio is limited by the need to design hairpins with stem structures long enough to minimize signal from non-bound probes, yet short enough to provide instability to allow probe–target hybridization within reasonable timescales. These design criteria have restricted the use of MBs in homogenous, single molecule assays,[12,18] where signals from thermally fluctuating MBs become indistinguishable from bound probes at low target concentrations, as shown in Fig. 4 and 5. Limitations such as these have led researchers to develop alternative FRET-based[11] and coincident[7,15,21] probe schemes specifically designed to increase signal-to-background ratios in single molecule studies.

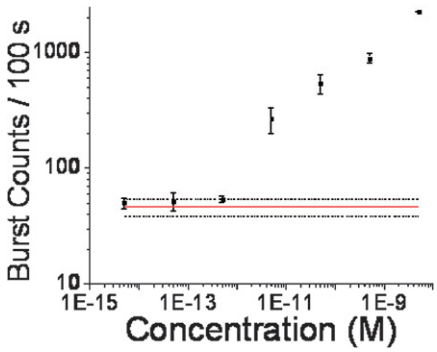

Fig. 4 Calibration curve of fluorescence burst counts *versus* target concentration loaded into the SMD rotary chamber[23] without evaporation-based accumulation (10 pM molecular beacon concentration). The solid line represents the average number of fluorescent bursts from the no target control (dotted line equals one standard deviation from an average of four measurements).

Still, probe–target reactions in these traditional SMD studies are typically conducted for hours prior to running confocal fluorescence detection experiments[13,15] and the overall sensitivity is still limited to fM.[11,15,21] These limits are due in part to the restricted molecular probe concentrations (nM–pM) required to maintain low levels of background fluorescence for SMD measurements, discussed previously. In addition, the long probe–target incubation times for SMD, extended read times reported to gain reliable results,[9,10,18] and difficulties in handling rare

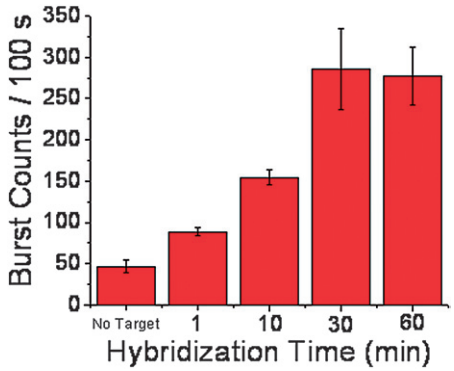

Fig. 5 Number of fluorescent bursts detected *versus* hybridization time (5 pM targets, 10 pM probe) within the device. Hybridization time follows a 15 s mixing period using the rotary pump and a 5 s incubation at 80 °C.

target molecules remain persistent barriers against more widespread use for quantification of biomolecules.[15] Fig. 5 shows the hybridization time required to obtain a maximum fluorescence burst count after loading 5 pM DNA targets into the microdevice. After mixing and hybridization, the MB signal saturates within a <30 min incubation time, significantly reducing the reaction time required for experiments in which target concentrations have been enhanced to this level, compared to direct quantification from dilute or sub-picomolar concentrations using traditional SMD platforms. Thus, the rate limiting step in fluorescent event counting assays within the evaporator–SMD microdevice becomes solvent removal, which is a controllable device parameter (Fig. 3).

The unique micro-evaporator coupling to single molecule assays allows direct analysis from microliter-sized, low abundant, purified DNA solutions eliminating additional sample handling, in which variability could be introduced when using traditional SMD platforms. Importantly, solvent removal remains a viable option for nucleic acid concentration since several nucleic acid isolation protocols allow for washing or desalting of DNA, including phenol extraction/ethanol precipitation or elution using glass beads.[38] Re-suspension in purified water does not alter DNA integrity, while stringent cleaning protocols for the microdevice enables removal of large amounts of solvent for concentration factors reaching 1000's with little effect on subsequent hybridization reactions. In addition, probe introduction to the microdevice takes place following solvent removal from separate device inlets facilitating hybridization reactions within buffered and controlled conditions that are independent of the concentration step. This becomes especially important when using hairpin probes, such as molecular beacons, since several important probe properties, including signal-to-background ratio and specificity, are altered dramatically in solutions with differing ionic strengths.[34,37,39] Indeed, these requirements highlight the advantage of performing recirculating SMD[23] within a microdevice amenable to arrayed formats for probing optimal buffer conditions from concentrated sample plugs.

As shown in Fig. 2, target DNA is advected toward the dead-end valve during evaporation where it accumulates for subsequent transfer and detection within the SMD rotary chamber. The width of this accumulation zone is dependent on backwards thermal diffusion of the concentrated species.[30] As shown in Fig. 2C, the width of target accumulation is comparable to the

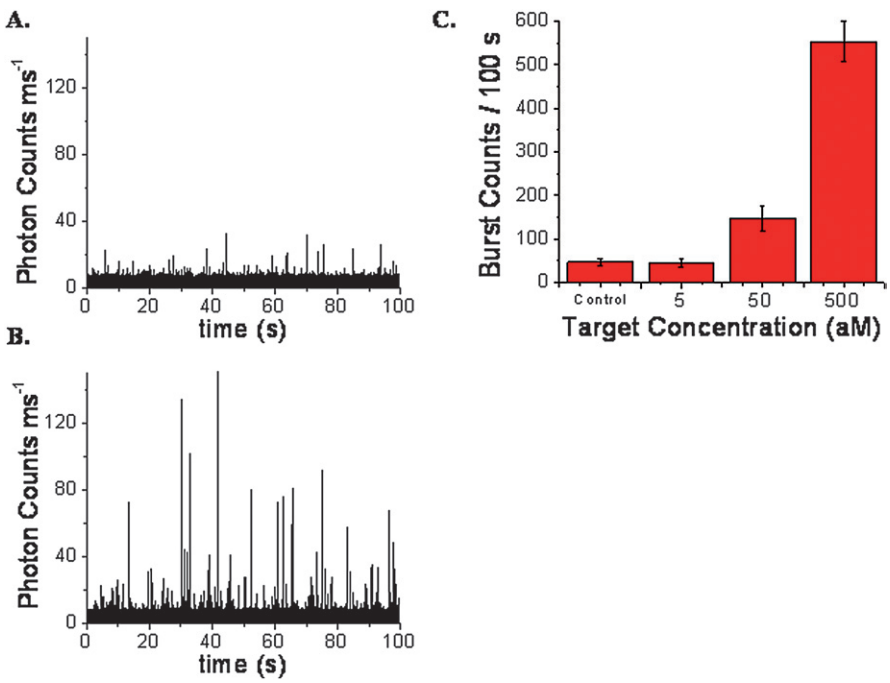

Fig. 6 **(A and B)** Raw fluorescence burst traces from the recirculating SMD chamber[23] (100 Hz pump frequency) after 20 hours of target enrichment and probe hybridization with no target control (A) and 50 aM target (B) samples. **(C)** Number of fluorescent bursts detected *versus* loading concentration after 20 hours of evaporation within the 1000 mm membrane device (10 pM probe, room temperature, 25 PSI), along with no target controls.

volume swept into the rotary pump for SMD; therefore, the rate of concentration within the microdevice is directly dependent on increase in target concentration within this accumulation zone. At large running times the growth of this accumulation zone can be estimated using the time scale associated with emptying one complete evaporator channel volume or $t_e = h/v_e$, where h is the height of the channel and v_e is the evaporation velocity through the pervaporation membrane.[30] Evaporation velocity is calculated over the total pervaporation surface (S) as $v_e = Q_e/S$, where Q_e is the measured volumetric flow rate achieved through solvent removal. Evaporation at 25 PSI nitrogen pressure results in an estimated Q_e of 21.63 nL min^{-1}, as shown above, giving a t_e value of ~55 min and a target flux of $J = Cv_e$ within that time, where C represents the concentration of target within the sample reservoir. At this rate of evaporation the longest concentration time attempted in this report resulted in removal of ~26 μL of solvent or a ~6500-fold enhancement in target concentration within the four nanoliter SMD chamber. In the MB calibration curve (Fig. 4), the pM level burst count response above background reveals that the above level of target enhancement would yield theoretical detection limits approaching 200 aM after solvent removal. Indeed, Fig. 6 validates this aM level detection limit after evaporation, showing a measured limit of 50 aM after evaporation. The 4-fold descrepancy between the measured and expected detection limits may be attributable to chip-to-chip variations in evaporation rates due to membrane thickness or alignment. In addition, while the evaporation coil may serve as an interconnect to large clinical sample volumes, the dilute DNA solutions used in this report must be prepared through serial dilutions and are subject to pipetting errors. Still, as shown the enrichment of the 100s of target molecules (Fig. 6B) from the aM sample was sufficient for detection above the background fluorescent bursts (Fig. 6A) resulting from thermal fluctuations of the 1000s of MB probes injected into the SMD chamber. These results demonstrate efficient transport of the low abundant DNA molecules through the relatively inert PDMS evaporator. Furthermore, it is noteworthy that enumeration of these few hundred molecules ferried to the four nanoliter SMD chamber would still pose quite a challenge were it not for the application of recirculating confocal fluorescence detection.[23] Resampling within the discrete nanoliter chamber enables utilization of the majority of the molecular information contained in the SMD chamber in relatively short read times, thus permitting the unique combination of an evaporation-based concentrator and SMD. In addition, Fig. 3 shows that modification of simple operating parameters explored in this report lead to Q_e values of 100's nanoliters per minute, showing that the evaporation time necessary for achieving these detection limits can be drastically reduced. Even so, to our knowledge this represents the first practical report of attomolar sensitivity using single molecule fluorescence counting or common hairpin probes.

4 Conclusions

Novel means of analyte delivery are necessary in order to breach the common femtomolar detection limits in current microfluidic platforms.[13,15,40,41] Micro-evaporators represent a unique method to bridge the gap between real world, microliter biological samples and the nano- to picoliter detection volumes within microanalytical systems. Specifically, the well-controlled evaporation rates within microdevices[28] enable highly reproducible transfer of a small number of molecular targets to specified detection components within microfluidic networks. In this report, DNA targets are detected at initial concentrations as low as 50 aM using a simple hairpin probe. Thus, the novel scheme of using solvent removal for analyte transfer to a nanoliter-sized detection volume not only obviates the need for special fluorescent probes designed specifically for confocal fluorescence detection, but surpasses the detection limits of these probes used in normal microfluidic platforms.[9,11,13,15] Key to this result is performing single molecule fluorescence detection within a closed-loop rotary pump,[23] which decreases the hybridization assay volume by orders of magnitude, thus allowing direct coupling to the microfluidic evaporator. In addition, detection is made from the typical starting volumes normally handled with pipettes and bench-top processing techniques, rendering the microdevice compatible with common nucleic acid isolation procedures, such as alcohol precipitation[38] and affinity-based separation, which result in re-suspension of small amounts of DNA in microliters of water.

Micro-evaporators could easily be integrated with other detection schemes, such as disk and wire-like nano-biosensors[40–43] to increase analyte transfer and kinetics of target capture. Detection chambers for these nanoscale biosensors could reach picoliter levels, enabling concentration factors surpassing the ~6500 shown using nanoliter chambers in this report. Indeed, optimization and standardization of micro-evaporators as universal analyte inputs to microanalytical systems could lift many of the current limitations of conventional microfluidic delivery systems.[40,41] Additional improvements to membrane-based evaporators could include ion permeable membranes, enabling control over buffer concentrations during solvent removal, thus expanding applicability to complex protein- and microorganism-containing samples. Further modifications to the evaporator coil could also include the use of three-dimensional microstructures to maximize the surface area of the pevaporation membrane, which would lead to increases in assay sensitivity, while substantially decreasing total processing time. In this manner, processing times for SMD platforms, such as single molecule fluorescence counting, that are traditionally limited due to probe–target hybridization kinetics would become dominated by the controllable evaporation or enrichment speeds within the evaporation-based analyte input. In addition, utilizing solvent removal as a simple method of analyte transport alleviates many of the challenges involved with low-volume sample processing and the lack of compatibility between conventional lab methodologies and SMD. Therefore, these results represent a clear example that for specific biological applications the performance of any microanalytical device must be assessed by the sensitivity of the sum of its parts, and not just the responsivity of its probe.

Acknowledgements

The authors would like to thank H. C. Yeh, Y. P. Ho, K. Liu, and T. Rane for advice and technical support throughout this work. The authors would also like to acknowledge funding support from the NSF, NIH, and DARPA.

References

1 J. Melin and S. R. Quake, *Annu. Rev. Biophys. Biomol. Struct.*, 2007, **36**, 213–231, DOI: 10.1146/annurev.biophys.36.040306.132646.
2 S. Y. Teh, R. Lin, L. H. Hung and A. P. Lee, *Lab. Chip*, 2008, **8**, 198–220, DOI: 10.1039/b715524g.
3 S. Haeberle and R. Zengerle, *Lab. Chip*, 2007, **7**, 1094–1110, DOI: 10.1039/b706364b.
4 H. Craighead, *Nature*, 2006, **442**, 387–393, DOI: 10.1038/nature05061.
5 A. J. de Mello, *Lab. Chip*, 2003, **3**, 29N–34N, DOI: 10.1039/b304585b.
6 A. G. Crevillen, M. Hervas, M. A. Lopez, M. C. Gonzalez and A. Escarpa, *Talanta*, 2007, **74**, 342–357, DOI: 10.1016/j.talanta.2007.10.019.
7 A. Castro and J. G. Williams, *Anal. Chem.*, 1997, **69**, 3915–3920.
8 J. P. Knemeyer, N. Marme and M. Sauer, *Anal. Chem.*, 2000, **72**, 3717–3724.
9 H. Li, L. Ying, J. J. Green, S. Balasubramanian and D. Klenerman, *Anal. Chem.*, 2003, **75**, 1664–1670.
10 H. Li, D. Zhou, H. Browne, S. Balasubramanian and D. Klenerman, *Anal. Chem.*, 2004, **76**, 4446–4451, DOI: 10.1021/ac049512c.
11 C. Y. Zhang, H. C. Yeh, M. T. Kuroki and T. H. Wang, *Nat. Mater.*, 2005, **4**, 826–831.
12 C. Y. Zhang, S. Y. Chao and T. H. Wang, *Analyst*, 2005, **130**, 483–488, DOI: 10.1039/b415758c.
13 L. A. Neely, S. Patel, J. Garver, M. Gallo, M. Hackett, S. McLaughlin, M. Nadel, J. Harris, S. Gullans and J. Rooke, *Nat. Methods*, 2006, **3**, 41–46, DOI: 10.1038/nmeth825.
14 H. C. Yeh, Y. P. Ho, I. Shih and T. H. Wang, *Nucleic Acids Res.*, 2006, **34**, e35, DOI: 10.1093/nar/gkl021, 34/5/e35 [pii].
15 C. M. D'Antoni, M. Fuchs, J. L. Harris, H. P. Ko, R. E. Meyer, M. E. Nadel, J. D. Randall, J. E. Rooke and E. A. Nalefski, *Anal. Biochem.*, 2006, **352**, 97–109, DOI: 10.1016/j.ab.2006.01.031.
16 N. Marme and J. P. Knemeyer, *Anal. Bioanal Chem.*, 2007, **388**, 1075–1085, DOI: 10.1007/s00216-007-1365-1.
17 H. C. Yeh, C. M. Puleo, Y. P. Ho, V. J. Bailey, T. C. Lim, K. Liu and T. H. Wang, *Biophys. J.*, 2008, **95**, 729–737, DOI: 10.1529/biophysj.107.127530.
18 T. H. Wang, Y. Peng, C. Zhang, P. K. Wong and C. M. Ho, *J. Am. Chem. Soc.*, 2005, **127**, 5354–5359, DOI: 10.1021/ja042642i.
19 H. C. Yeh, S. Y. Chao, Y. P. Ho and T. H. Wang, *Curr. Pharm. Biotechnol.*, 2005, **6**, 453–461.
20 H. C. Yeh, Y. P. Ho and T. H. Wang, *Nanomedicine*, 2005, **1**, 115–121, DOI: 10.1016/j.nano.2005.03.004.
21 R. L. Nolan, H. Cai, J. P. Nolan and P. M. Goodwin, *Anal. Chem.*, 2003, **75**, 6236–6243.
22 H. P. Chou, M. A. Unger and S. Quake, *Biomed. Microdevices*, 2001, **3**, 323–330.
23 C. M. Puleo, H. C. Yeh, K. J. Liu and T. H. Wang, *Lab Chip*, 2008, **8**, 822–825, DOI: 10.1039/b717941c.
24 Y. S. Heo, L. M. Cabrera, J. W. Song, N. Futai, Y. C. Tung, G. D. Smith and S. Takayama, *Anal. Chem.*, 2007, **79**, 1126–1134, DOI: 10.1021/ac061990v.
25 G. C. Randall and P. S. Doyle, *Proc. Natl. Acad. Sci. USA*, 2005, **102**, 10813–10818, DOI: 10.1073/pnas.0503287102.
26 J. Leng, M. Joanicot and A. Adjari, *Langmuir*, 2007, **23**, 2315–2317.
27 G. M. Walker and D. J. Beebe, *Lab. Chip*, 2002, **2**, 57–61, DOI: 10.1039/b202473j.
28 M. Zimmermann, S. Bentley, H. Schmid, P. Hunziker and E. Delamarche, *Lab. Chip*, 2005, **5**, 1355–1359, DOI: 10.1039/b510044e.
29 M. A. Unger, H. P. Chou, T. Thorsen, A. Scherer and S. R. Quake, *Science*, 2000, **288**, 113–116, (DOI:8400 [pii]).
30 J. Leng, B. Lonetti, P. Tabeling, M. Joanicot and A. Ajdari, *Phys. Rev. Lett.*, 2006, **96**, 084503.
31 S. Y. Chao, H. Yi-Ping, V. J. Bailey and T. H. Wang, *J. Fluoresc.*, 2007, **17**, 767–774.
32 J. Enderlein, D. Robbins, W. Ambrose and R. Keller, *J. Phys. Chem. A*, 1998, **102**, 6089–6094.
33 R. C. Habbersett and J. H. Jett, *Cyto. A*, 2004, **60A**, 125–134.
34 C. Xi, L. Raskin and S. A. Boppart, *Biomed. Microdev.*, 2005, **7**, 7–12.
35 Genevac, Ltd., *EZ-Bio, Second Generation Evaporation/Concentration System for Life Science Laboratories*, www.genevac.com, 2008.
36 C. M. Puleo, H. C. Yeh, K. J. Liu, T. Rane and T. H. Wang, MEMS 2008. IEEE 21st International Conference on Micro Electro Mechanical Systems, pp. 200–203.
37 A. Tsourkas, M. A. Behlke, S. D. Rose and G. Bao, *Nucleic Acids Res*, 31, 1319–1330.
38 D. Moore, *Purification and concentration of DNA from aqueous solutions*. Curr Protoc Immunol. 2001, pp. 10.1.
39 Z. Tang, K. Wang, W. Tan, J. Li, L. Liu, Q. Guo, X. Meng, C. Ma and S. Huang, *Nucleic Acids Res.*, 2003, **31**, e148.
40 P. R. Nair and M. A. Alam, *Appl. Phys. Lett.*, 2006, **88**, 233120.
41 P. E. Sheehan and L. J. Whitman, *Nano Lett.*, 2005, **5**, 803–807, DOI: 10.1021/nl050298x.
42 Z. Gao, A. Agarwal, A. D. Trigg, N. Singh, C. Fang, C. H. Tung, Y. Fan, K. D. Buddharaju and J. Kong, *Anal. Chem.*, 2007, **79**, 3291–3297.
43 F. Patolsky, G. Zheng and C. M. Lieber, *Nanomed.*, 2006, **1**, 51–65.

